Hindawi
International Journal of Aerospace Engineering
Volume 2019, Article ID 5194268, 11 pages
https://doi.org/10.1155/2019/5194268

Research Article

Study of Manufacturing Process of Holes in Aeroengine Heat Shield

Anyuan Jiao [1,2] **and Weijun Liu** [3]

[1]*School of Mechanical Engineering and Automation, Northeastern University, Shenyang 110819, China*
[2]*School of Applied Technology, University of Science and Technology Liaoning, Anshan 114002, China*
[3]*School of Mechanical Engineering, Shenyang University of Technology, Shenyang 110870, China*

Correspondence should be addressed to Weijun Liu; liuwj@huiyuanrobot.com

Received 11 April 2019; Accepted 11 July 2019; Published 14 August 2019

Academic Editor: Giacomo V. Iungo

The nickel-based superalloy GH3128 with high plasticity, high long-lasting creep strength, good resistance to oxidation and stamping, and good welding performance is widely used in aircraft engine heat shields. The many holes that need to be machined on the heat shield are not only small in diameter but also dense, and GH3128 as a typical hard-to-process material has the problems of large cutting force, high cutting temperature, and serious hardening. Therefore, poor dimensional accuracy and residual burrs have become the main factors that limit the processing efficiency and processing quality. So, a novel combination of manufacturing processes was proposed. Firstly, laser cutting technology was used to process the base hole in a GH3128 plate, followed by reaming, and finally, using a magnetic abrasive finishing effector to remove burrs formed during the first two steps. The whole drilling process of the heat shields fully meets the requirements of the technical parameters. This study provides new reference for manufacturing the holes of a heat shield and other similar porous parts.

1. Introduction

GH3128 is a nickel-based superalloy with a solid solution of tungsten and molybdenum and is reinforced with boron, niobium, and zirconium. Ezugwu et al. in 2003 [1] pointed out that the nickel-based superalloy was the most widely used alloy, accounting for about 50 wt.% of materials used in an aerospace engine. Li in 2016 [2] also mentioned that GH3128 was used in an aircraft engine combustor flame tube, an afterburner housing, an adjusting plate, and in other high temperature parts. The afterburner of an aeroengine is equipped with a corrugated heat shield made of GH3128 material, which has many film holes on it to prevent the combustion chamber from overheating and oscillating. There are many holes in the heat shield that are densely arranged. Due to the small diameter and the higher position accuracy of these holes, it is difficult to create them using the traditional punching or drilling process in this thin-walled surface. Generally, precision punching, electrical discharge machining (EDM), or laser cutting technology was used for manufacturing thin-walled holes. Precision punching equipment is very expensive, and it has many limits for the shape and size of the workpiece. In addition, the process needs to manufacture special molds corresponding to different workpieces and the cost of mold is also expensive. Xu et al. in 2009 [3] mentioned that the materials with a high specific strength are generally machined using EDM, and five material-removal mechanisms of cemented carbides machined by ultrasonic vibration-assisted EDM are proposed, which are melting and evaporation, oxidation and decomposition, spalling, the force of high-pressure gas, and the affection of ultrasonic vibration. Moreover, there were microcracks on the cut surface; microcracks depend not only on electrical discharge parameters but also on the properties of a workpiece. D'Urso et al. in 2014 [4] mentioned that EDM is suitable for the machining of hard and high-strength materials, and they studied the process performance of micro-EDM drilling of stainless steel. High electrical conductivity results in a faster drilling process but in a lower dimensional and geometrical precision of the holes; the processing efficiency

Table 1: Chemical composition of GH3128 (wt.%).

Ni	Cr	W	Mo	Al	Ti	Fe	B	Zr	Ce
Bal	19.0~22.0	7.5~9.0	7.5~9.0	0.4~0.8	0.4~0.8	1.0	0.005	0.04	0.05

of EDM is relatively low. Sun in 2013 [5] confirmed that picosecond laser trepanning drilling of the directional solidification of a Ni_3Al-based superalloy has been studied, and the experiment demonstrates that there are periodic stripes in the hole wall. Ko et al. in 2003 [6] claimed that the step drill performs front edge cutting before step edge cutting, and the burr formed during the first cutting can be removed during the second cutting by step edge. In conclusion, these conventional processing schemes generally suffer from problems such as expensive manufacturing cost, poor versatility, poor hole-positioning accuracy, microcracks on the wall of the hole, or low processing efficiency. And Huang et al. in 2010 [7] confirmed that if these processes are used alone, the hole-making technical requirements of the heat shield cannot be well satisfied, too.

This paper is aimed at manufacturing qualified holes in a heat shield with more than 1 m in diameter and with a corrugate profile. Made of GH3128 with a wall thickness of 0.8 mm, a total of 4200 holes with a diameter of Ø5 mm are required. The technical requirement is that the diameter deviation of the holes is ±0.1 mm, the positional accuracy of the hole is ±0.1 mm, there are no burrs at the hole exit, and the edge fillet of the hole is ≤0.2 mm. Because of large size and complex shape of the heat shield, it is difficult to manufacture the hole and meet all of technical requirements using a conventional drilling process. In summary, a novel combination process composed of three steps is proposed: (1) the base hole (diameter is 4.2 mm) is created using the laser cutting method; (2) reaming (diameter is 5 mm) is performed; and (3) burr removal is accomplished by the magnetic abrasive finishing method. The novel process was proposed for achieving the goal of making qualified holes in a heat shield.

2. Experimental Study on Cutting the Base Hole

The principle of making a hole by laser is based on the synthesis process of high temperature melting and shock wave induced by the photothermal effect. Through a series of optical focusing systems, fine beams of high parallelism are generated, resulting in the lattice vibration of materials bombarded by extremely high-energy and high-density photon beams. Instantly, the light energy can be converted into heat energy, and the irradiated area will be heated up rapidly. Bai in 2015 [8] has stated that the material will undergo metallographic changes, melting, gasification, and considerable thermal stress in order to achieve the purpose of removing the material. The material at its focal point is exposed to a high-power high-density laser spot, which produces a local high temperature of 10000°C or more. The material vaporizes instantaneously, and the vaporized metal is blown away with the auxiliary cutting gas, cutting the material into a small size. As the focus moves, numerous microholes are connected to complete the cutting process. Meng in 2011 [9] built a vaporization-melt ratio mathematical model for improving of the quality in laser cutting of 6063 aluminum sheets with a thickness of 0.5 mm. The analysis verifies that the model is feasible, and it makes a contribution to laser precision cutting. Lei et al. in 2009 [10] mentioned that the laser cutting of a 0.5 mm silicon steel sheet with a CO_2 laser has been studied. Although neither reference mentions the GH3128 plate, it is all about laser-cut sheet metal. It can be seen that the laser cutting of GH3128 should be equally feasible. A 400 W Nd:YAG ($\lambda = 1064$ nm) laser was used to manufacture Ø4.2 mm holes in a GH3128 sheet with a thickness of 0.8 mm. Its matrix is austenite, and its main chemical compositions are shown in Table 1.

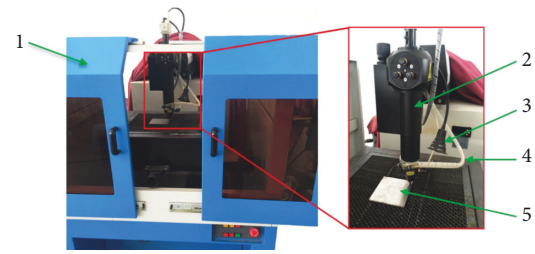

Figure 1: The appearance of laser cutting equipment (1—machine housing, 2—laser lens assembly, 3—lighting, 4—conveying pipe of auxiliary gas, and 5—workpiece).

3. Experimental Equipment and Procedures of Base Hole

The laser cutting equipment JHM-1GY-400B is shown in Figure 1. The specific parameters were as follows: the laser wave length is 1.06 μm, the rated average power of the laser is 400 W, and the laser pulse frequency is 1-200 Hz (adjustable). The laser pulse width is 0.1-20 ms (adjustable). The focal length of the lens is 75 mm, and the diameter of the focal spot is 0.3-0.6 mm. O_2 was used as the auxiliary gas.

Chen et al. in 2017 [11] aimed to analyze the effect of laser power, scanning speed, and processing times on the surface roughness of polymethyl-methacrylate microchannels with a CO_2 laser LCJG-1290 cutting process. Arun and Avanish in 2013 [12] investigated the laser cutting performance of a 1 mm duralumin sheet with the aim to improve the quality of the cut by simultaneously optimizing multiple performances such as cut edge surface roughness, kerf taper, and kerf width. Aoud et al. in 2017 [13] focused on evaluating the effect of laser power, cutting speed, and gas pressure on the heat-affected zone and kerf width quality. Gvozdev et al. in 2015 [14] built mathematical models that provide an adequate description of the effect of laser cutting parameters on the roughness of the cut surface with no burr and the extent of the heat-affected area, and the lack of perpendicularity of the cut surface was ascertained. By summarizing the

Table 2: Five-factor four-level orthogonal table.

Factors Level Name	Defocusing distance (mm) **A**	Cutting speed (mm/min) **B**	Current (A) **C**	Pulse width (ms) **D**	Frequency (Hz) **E**
1	-1.0	100	190	0.8	70
2	-0.75	150	200	0.9	75
3	-0.5	200	210	1.0	80
4	-0.25	250	220	1.1	85

references on these laser cuttings, the main technical parameters were selected and the experimental steps in this paper are proposed as follow: First of all, according to the references of relevant laser cutting, five technological factors, such as defocusing distance—**A** (mm), processing speed or cutting speed—**B** (mm/min), current—**C** (A), pulse width—**D** (mm), and frequency—**E** (Hz), were selected as the test parameters. The orthogonal test method of four levels and five factors $L_{16}(4^5)$ was developed, as shown in Table 2. The process parameters corresponding to the 16 sets of experimental data were obtained. Then, the base hole was made by the laser cutting process according to the technological parameters. Lastly, the results of the orthogonal experiment and the analysis of the variance were done.

4. Intuitive Analysis

The comprehensive evaluation index V_A was formulated as shown in

$$V_A = \left(100 - \frac{h}{20}\right) \times \frac{l}{L}, \quad (1)$$

where h is the slag thickness (mm), l is the cut length (mm), and L is the total length of the cut (mm). $(l/L \times 100\%)$ is the cut ratio. The slag thickness at the hole entrance by the laser cutting method was smaller relative to that at the exit. Therefore, the slag thickness of the hole exit was only detected and analyzed. The thickness values of six points were measured, and the mean value of the slag thickness was calculated. The experimental data are shown in Table 3.

The best results were No. 8 and No. 16, and the slag thickness was 280 μm; the worst results were No. 4, No. 5, No. 6, and No. 9, and all holes did not penetrate the alloy plates as shown in Figure 2. It could be seen from the test photo of No. 4 that the reason for the uncut was that the starting point was not cut, which belonged to the early to middle part of the cutting. The first condition of laser cutting was that the starting point penetrates to form a keyhole effect, so that the material had a 100% absorption rate of the laser. The probability of cutting completeness was significantly increased. Therefore, it was necessary to stay at the cutting starting point to meet the above requirements. Then, the starting point did not cut the laser power density of the process parameters, which was insufficient in the stay time. When the laser power accumulated enough, it could indeed penetrate the plate. However, due to the movement of the numerical control platform, the instability of the laser and air pressure caused to the slag to be poor and thus causing the cutting failure.

Table 3: Comprehensive evaluation table of orthogonal test.

No.	Test conditions (**A**, **B**, **C**, **D**, and **E**)	Slag thickness (μm)	Cut the proportion (%)	Comprehensive score (V_A)
1	11111	480	100	76
2	12222	500	100	75
3	13333	380	100	81
4	14444	500	37.5	28
5	21234	450	25	19
6	22143	500	25	18
7	23412	400	100	80
8	24321	280	100	86
9	31342	420	37.5	29
10	32431	420	100	79
11	33124	360	100	82
12	34213	320	100	84
13	41423	460	100	77
14	42314	400	100	80
15	43241	420	100	79
16	44132	280	100	86

The data in Table 3 was analyzed, and the specific steps were as follows: (1) Summarize the values of level 1, level 2, level 3, and level 4 and use $\mathbf{A}_j$, $\mathbf{B}_j$, $\mathbf{C}_j$, $\mathbf{D}_j$, and $\mathbf{E}_j$ (j is the representative level) to form them. (2) The average value of each factor was calculated, i.e., $\mathbf{A}_j/4$, $\mathbf{B}_j/4$, $\mathbf{C}_j/4$, $\mathbf{D}_j/4$, and $\mathbf{E}_j/4$. (3) The difference (R_j) between the maximum or the minimum was calculated separately. It was called the extreme difference. The analysis results are shown in Table 4.

According to the R_j value, the influence of each factor on the experiment result could be judged. In Table 4, the extreme difference was the maximum difference between the mean value, and the range of the difference represented the degree of influence of this factor on the laser cutting process. The larger the difference, the more important it was. Thus, the order of the main and secondary factors could be determined. Therefore, the effect of the five factors on laser perforation was obtained: **D** > **B** > **A** > **E** > **C**. In order to more vividly and more intuitively draw the analysis results, the method of drawing effect plots (trends) was adopted to get the correct comprehensive analysis

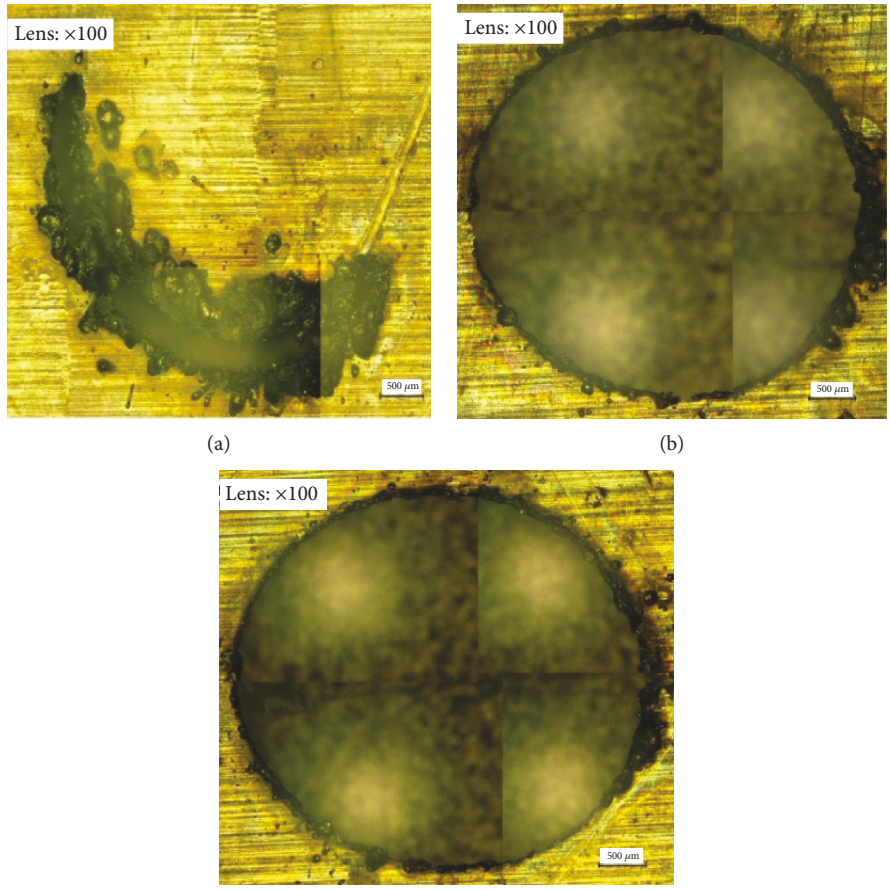

Figure 2: Slag photos of hole exit at ×100 magnification (No. 4 (a), No. 8 (b), and No. 16 (c)).

Table 4: Analysis table of orthogonal test.

Factors Level	A	B	C	D	E
Level 1 mean	65	50.25	65.50	80	80
Level 2 mean	50.75	63	64.25	80	67.5
Level 3 mean	68.50	80.50	69	66.25	65
Level 4 mean	80.50	71	66	38.5	52.25
Extreme difference R_j	29.75	30.25	4.75	41.5	27.75

conclusion. According to the mean value of four levels in Table 4, the effect curve was obtained, as shown in Figure 3. The optimum **A** was -0.25 mm. The reason was that the closer one gets to the focal point, the greater was the laser power density and the better was the cutting ability and the cutting quality. Or, in the case of ensuring the power density, the increase of the distance from the coke would inevitably increase the spot size, so that the width of the slit widens to eliminate the slag. This was also the reason why the cutting quality when out of focus at -1 mm was better than that at -0.75 mm. The best **B** was 200 mm/min; too low processing speed and too high energy density led to a poor slag, while too high processing speed and too low energy density led to poor cutting ability. The optimum **C** was 210 A; when the current level was within the range of 190-220 A, it had no significant effect on cutting quality. The optimum **D** was 0.8 ms and 0.9 ms. As the pulse width continued to increase, it would cause each laser pulse to accumulate excessive heat and accumulate too much slag. The optimal **E** was 70 Hz. Excessively high frequencies will result in too many laser cuts, excessive heat accumulation, and severe slag levels. The optimum process parameters could be obtained by taking the best horizontal value of each factor: **A** = −0.25 mm; **B** = 200 mm/min; **C** = 210 A; **D** = 0.8 ms or 0.9 ms; and **E** = 70 Hz.

5. Analysis of Variance

In order to further verify the experimental results of the intuitionistic analysis, the analysis of variance (ANOVA) for the experimental data is carried out:

$$C = \frac{T^2}{n}. \tag{2}$$

where C is the number of corrections; n is the total number of trials, which is 16; and T is the sum of 16 test scores. The total sum of squares of the variance of the test should be the sum of the variance squared of each factor and error, because

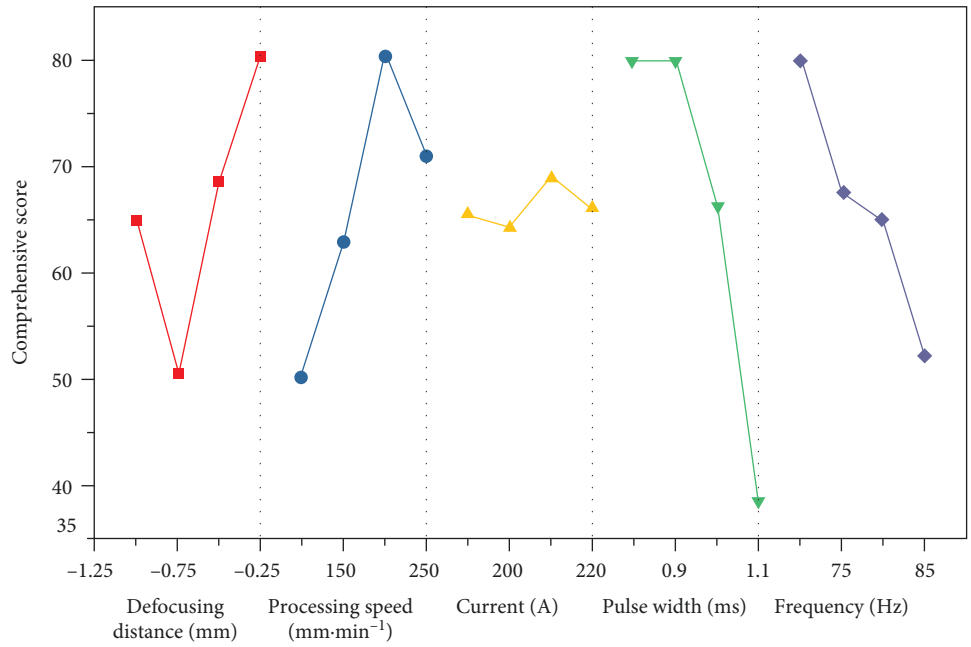

Figure 3: The effect curve of horizontal degree.

Table 5: Variance analysis table.

Factors	Sum of squares of variance (S_i)	Degrees of freedom (df_i)	F-ratio	$F0.01$ critical value	Significant
A	1800	3	36.73	29.5	*
B	1969	3	40.18	29.5	*
C	49	3	1	29.5	
D	4593	3	93.73	29.5	**
E	1553	3	31.69	29.5	*
Error	49	3			

Note: C is used as the error term. The F-ratio in the table is the ratio of the squared sum of the variance of each factor and the error. The critical value of the F-ratio greater than $F0.01$ is significant. According to the size of the F-ratio, the influence degree of each factor on the quality of laser cutting is obtained as follows: **D** > **B** > **A** > **E** > **C**. The conclusion of the ANOVA was consistent with the result obtained in Table 4 in the intuitive analysis, which further proves the correctness of the intuitive analysis. It can be seen in Table 5 that **A**, **B**, **D**, and **E** play a leading role in the laser cutting process, and they do not interfere with test error and interaction. The effect of current was not significant compared with the other four parameters; however, it is consistent with current floating with the intuitive analysis.

the test factors fill the entire orthogonal table; there is no empty column and there is no error term in the variance analysis. In fact, the error term is an unmeasured null column, so the choice of the least factor of the influence factor as the error term can also be used to compare the significant effect.

$$S = S_A + S_B + S_C + S_D + S_E + S_e, \tag{3}$$

where S is the sum of the squares of variance; S_A is the sum of the variance of **A**, S_B is the sum of the variance of **B**, and so on for S_C, S_D, and S_E (the specific representative factors of **A**, **B**, **C**, **D**, and **E** are shown in Table 2); and S_e is the sum of the squared error variance.

$$S = \sum X_j^2 - C, \tag{4}$$

where X is a comprehensive test score and j is the test number (as shown in Table 3).

$$S_A = \sum \frac{T_A^2}{k_a - C}, \tag{5}$$

where T_A is the sum of all the horizontal test scores of the **A** factor; a is the horizontal number of **A**, b is the horizontal number of **B**, and so on for c, d, and e; k_a is the horizontal repetition number of **A**, k_b is the horizontal repetition number of **B**, and so on for k_c, k_d, and k_e; $a = b = c = d = e = 4$; and $k_a = k_b = k_c = k_d = k_e = 4$. Total freedom of the experiment is $df = n - 1$. The degree of freedom (DOF) of the **A** factor is $df_A = a - 1$. S_B, S_C, S_D, and S_E and df_B, df_C, df_D, and df_E are consistent with the meaning of S_A and df_A. The variance analysis results were calculated according to equation (3). The results are shown in Table 5.

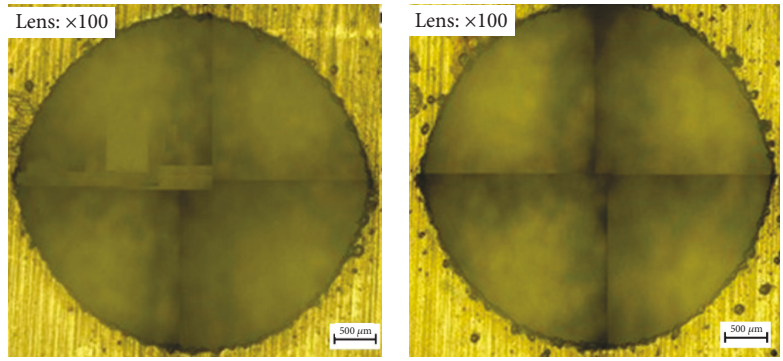

(a) (b)

Figure 4: Comparing photos (**D** = 0.8 ms (a) and **D** = 0.9 ms (b)).

Table 6: Comparison form of slag thickness.

Imaging area	Left	Right
D = 0.8 ms	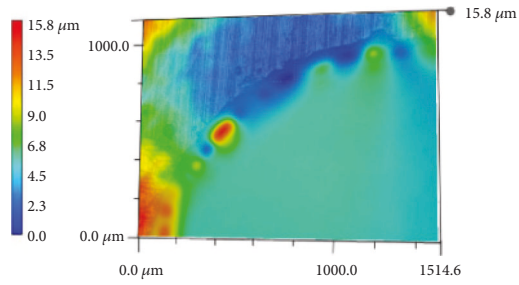	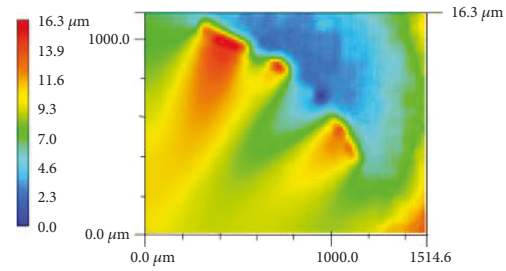
	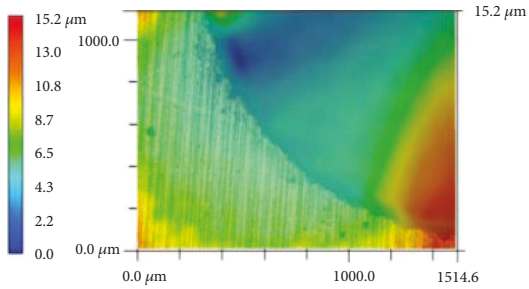	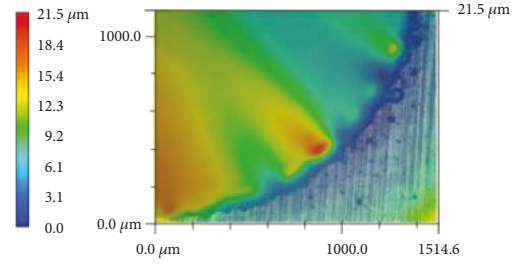
D = 0.9 ms	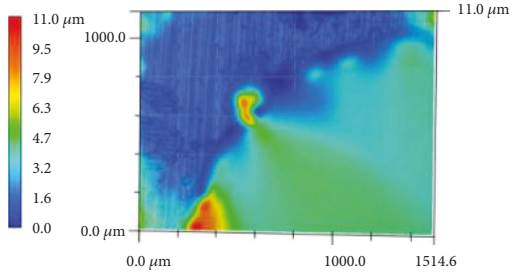	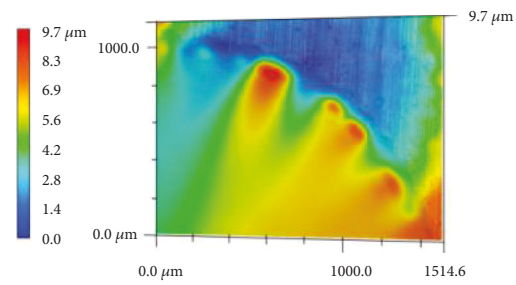
	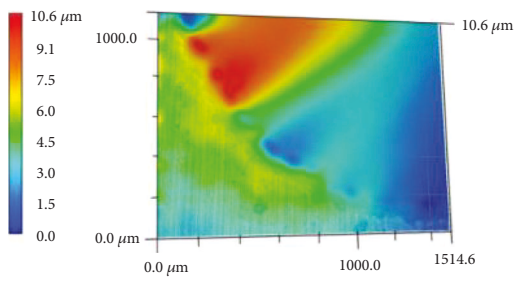	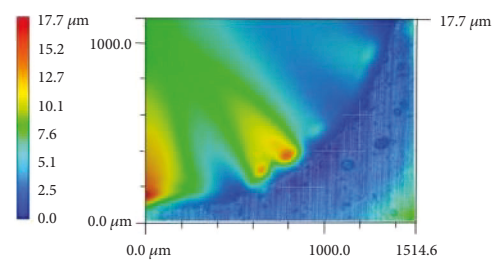

Table 7: Comprehensive evaluation table of validation experiment.

Test no.	Conditions (**A**, **B**, **C**, **D**, and **E**)	Slag thickness (μm)	Cut the proportion (%)	Comprehensive score (V_A)
17	43311	21.5	100	98.93
18	43321	17.7	100	99.12

6. Validation Experiment of Cutting Base Hole

It was shown that the optimum process parameters obtained by intuitionistic analysis could improve the number of laser-perforated slag. Because **D** = 0.8 ms or 0.9 ms, it was necessary to do two series of experiments to compare and obtain the best process parameters. The experiment results were measured and shown in Figure 4.

It was difficult to directly distinguish the slag level from macrophotos. Therefore, the KEYENCE VHX-500FE super-depth electron microscope was used to compare the slag thickness, as shown in Table 6.

From Table 6, it could be seen that the slag level in the right area of the entire hole photo was worse than elsewhere. The reason was the starting point of the laser cutting process at the right bottom side of the hole. Because at the beginning of the actual operation, it was necessary to stay at the starting point for a certain amount of time to stabilize the laser power and accumulate enough energy to form the small hole for the blackbody effect. Therefore, the slag was worst at the right bottom side of the hole at the beginning than at the other zones of the cutting. Similarly, the right side at the back was also a starting point, and the numerical control platform had an acceleration process from the starting point to the preset constant stable speed and there was a deceleration process at the end of the uniform state. The change in the moving speed of these two processes leads to the instability of the laser and air pressure, which makes the slag thickness poor. Therefore, the slag thickness near the starting point is poor. The process was as follows: the slag in the initial and accelerated stages of the cutting was poor, the number and height of the slag in the middle phase of cutting was gradual and steady, and the slag was poor during the deceleration stages of the cutting process. The top 6 slag areas around the whole hole were selected, and the height value was obtained through the software of the electron microscope. The difference between this value and the height of the workpiece was the thickness of the slag. As **D** = 0.8 ms or 0.9 ms, the mean values of the slag thickness were 21.5 μm and 17.7 μm, respectively. By taking this parameter into equation (1), we arrive at the calculation results as shown in Table 7.

From Table 7, it could be seen that the intuitive analysis could significantly improve the cutting quality. Test scores on both No. 17 and No. 18 were higher than those on No. 8 and No. 16 in Table 3. The test results of No. 18 were slightly better than those of No. 17. Therefore, the optimal process parameters were as follows: **A** = −0.25 mm; **B** = 200 mm/min; **C** = 210 A; **D** = 0.9 ms; and **E** = 70 Hz. It took 4.71 s to manufacture the Ø5 mm holes by the laser cutting process on a 0.8 mm thick GH3128 plate. After completing the manufacturing of one hole, the actuator was displaced and began to make the next hole. The moving speed of the actuator was 1000 mm/min, and the distance between the two holes was 12 mm, so it needed to take about 0.72 s to change to the next drilling position.

Table 8: The reaming process parameters.

Name	Parameters
Workpiece	GH3128, Ø$d1$ = 4.2 mm, δ = 0.8 mm
Whether a support plate or not	No
Drilling bit parameters	118° rake angle, material for HSS
Spindle speed	700 r/min
Quantity per tooth	f_Z = 0.05 mm
Cooling way	Natural cooling

7. Reaming

Using the integral alloy drilling bit with a 118° rake angle of HSS material, the base holes manufactured by optimized laser cutting process were reamed by a vertical milling machine. The diameter of the base hole was 4.2 mm, and the reamed diameter of the hole was 5 mm. The reaming process parameters are shown in Table 8.

After the hole was reamed, the burrs at the entrance edge of the hole were relatively small, and the naked eye could hardly detect it. But there were still burrs at the exit edge, and the detection methods and results are shown in Figure 5. Ten typically reamed holes were measured. The height of the burr was about 40-80 μm, and the width was between 132 and 300 μm. The height of the burr was significantly lower than that of the direct drilling process. The height and width were about 58.4% and 74.1%, respectively, compared to the direct drilling process. The main reason is that there is a larger axial pressure between the drill bit and the workpiece in the conventional process.

8. Deburred by MAF

The principle of magnetic abrasive finishing is to use a magnetic field to restrain magnetic abrasive particles to form magnetic brushes. Yun et al. in 2016 [15] aimed to improve the efficiency and uneven texture by using ultra-assisted MAF, and the study reveals that the efficiency of the surface roughness and material removal of alumina ceramic tubes were achieved. Lin et al. in 2007 [16] employed MAF to conduct free-form surface abrasion of stainless SUS304 material operations, and Ramax yielded an even lower value similar to that of the mirror surface. Verma et al. in 2017 [17] presented

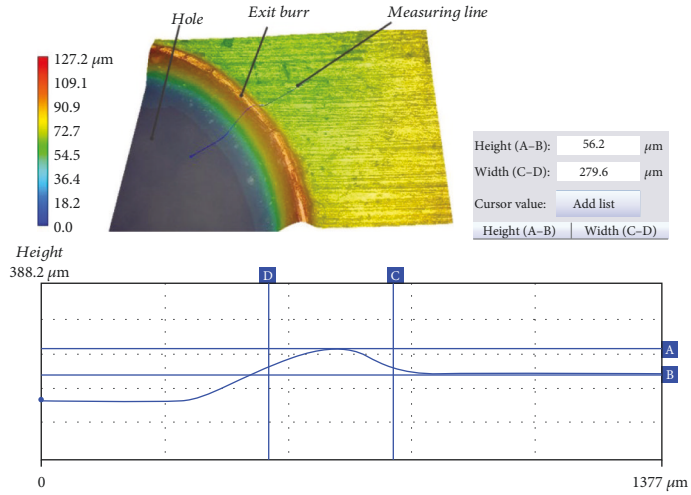

Figure 5: Measurement of the width and height of the burr at the hole exit.

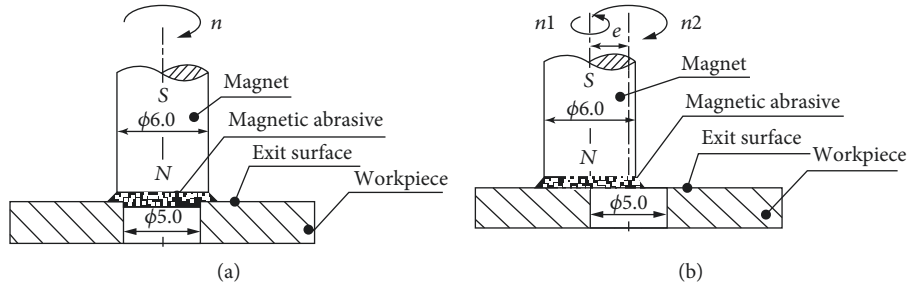

Figure 6: The principle comparison of the two plans (Plan 1 (a) and Plan 2 (b)).

experimental investigations into the internal MAF of SS304 pipes that resulted in a precise surface. Du et al. in 2015 [18] carried out large numbers of experiments on the electrolytic-MAF of the nickel-based superalloy GH4169, and the processing efficiency was improved. Moreover, Wang and Hu in 2005 [19] explained that the magnetic finishing process can also remove microcracks and have surface residual comprehensive stress, which can greatly improve the workpiece reliability and fatigue strength. The author of this paper, Jiao et al. in 2017 [20] pointed out that the relative motion between the magnetic brush and the burr is the main material-removal mechanism. After a comprehensive analysis of the mechanism of the magnetic finishing based on these references, the MAF process is feasible for the removal of burrs. The magnetic brush is flexible, and the reasonable design of the finishing pressure can completely avoid the deformation and will not cause new damage to the workpiece. The MAF method has many advantages, and many papers introduce the MAF principle for polishing pipes, plates, free-form surfaces, etc.; however, there is no related research on the edge deburring process for the hole exit. So in this paper, two kinds of plans based on MAF were proposed for burr removal after the reaming process. The principles are shown in Figure 6. Plan 1 is a magnetic pole self-rotation scheme. Here, the center axis of the magnetic pole is concentric to the center axis of the pass, the gap between the pole end and the workpiece is 2 mm, the magnetic particles fill in the gap, and the magnetic pole drives the magnetic particles to rotate clockwise. Compared with Plan 1, in Plan 2, the central axis of the magnetic pole deviates from the center axis of the hole. The magnetic pole rotates under its own rotation and revolves around the center of the hole. The specific process parameters are shown in Table 9. The height and width of the edge burr were detected every 30 s, and the average height value of the four higher typical burrs was calculated.

Table 9: Process parameters of the two plans.

Name	Plan 1	Plan 2
Workpiece	GH3128, $Ød = 5$ mm, $\delta = 0.8$ mm	
Abrasive	Self-made sintering abrasive, particle size 380 μm	
Finishing fluid	Oil grinding fluid	
Pole type	Cylindrical magnetic pole, $Ød = 6$ mm, $h = 30$ mm	
Working clearance	2 mm	
Spindle speed	1000 r/min	
Eccentricity	$e = 0$	$e = 5$ mm
Revolution (or speed)	Speed: 0 mm/min	Speed: 94.2 mm/min
Finishing time	3 min	

Using Plan 2 after 60 s, burrs were almost removed clearly. The micrographs after 60 s of processing with Plan 2 are shown in Table 10. There was no significant difference

Table 10: The contrast photos before and after finishing using Plan 2.

Imaging area	Left	Right
Before finishing	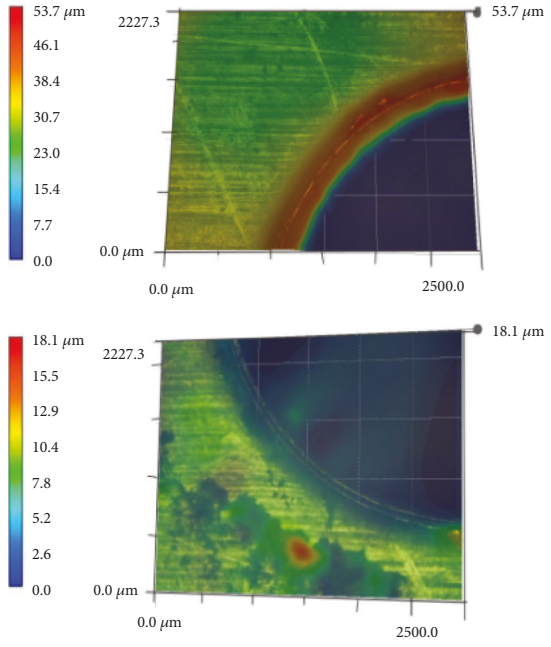	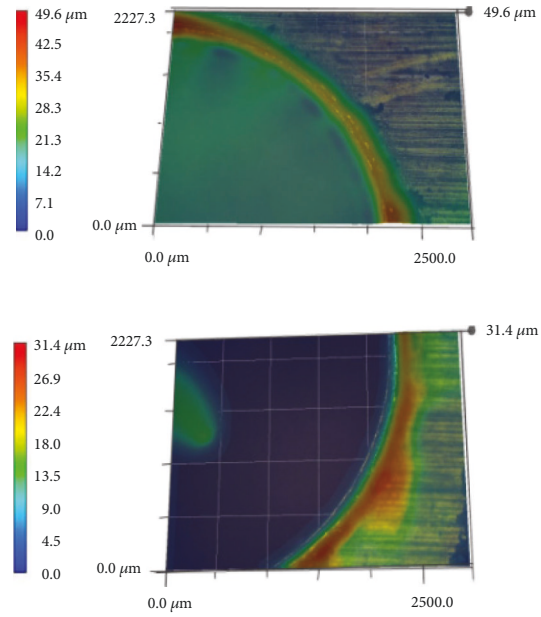
After finishing	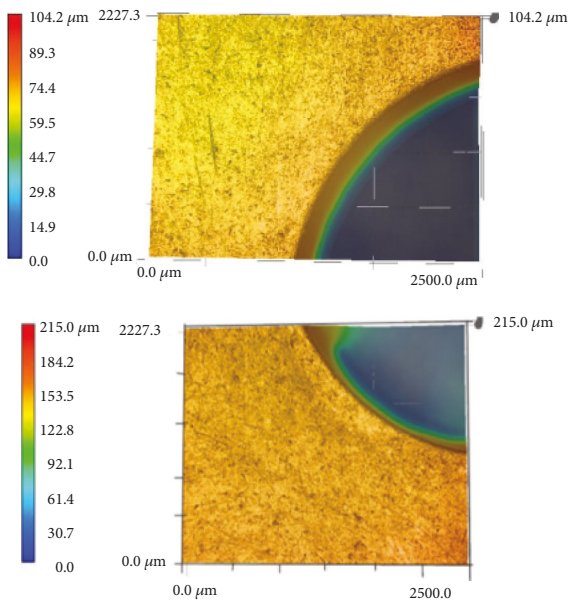	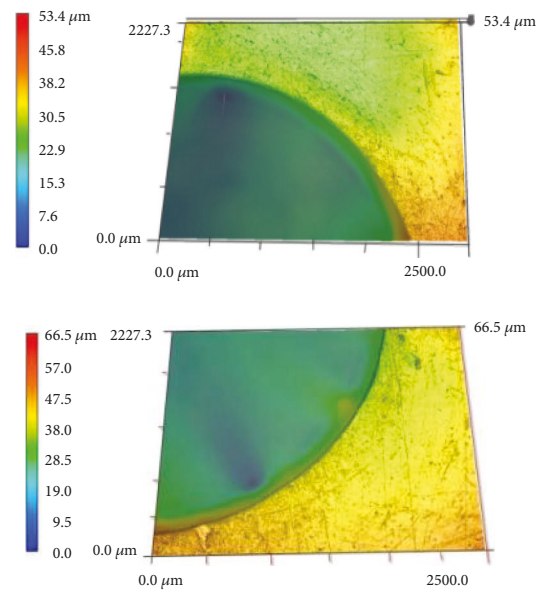

in the final effect between the two plans. But when comparing the edge burr removal efficiency, when Plan 2 was adopted, the removal efficiency of the edge burr was three times that of Plan 1, as shown in Figure 7. It could be seen from the form that the removal effect of the edge burr could meet the technical requirements. Liu et al. in 2014 [21] pointed out that the specialized tool can machine titanium holes without the burr based on a helical milling specialized tool. Wang et al. in 2018 [22] investigated cutting parameters in the helical milling process of a carbon fiber reinforced polymer. Li et al. in 2017 [23] analyzed the reason for reducing the hole exit defects by helical milling and grinding. Lu et al. in 2016 [24] built the dynamical model of the micro-milling process of a nickel-based superalloy. Based on these references, the helical milling process has been the focus of deburring research. But the direct contact between the tool and the workpiece causes damage and deformation easily. A major advantage of the magnetic abrasive finishing process is that the magnetic brush keeps a flexible contact with the workpiece, which can well avoid these defects. The test result shows that the complex motion of the particles accelerates the removal of the burrs. In other words, the adoption of the revolution leads the force of the magnetic brush on the burr to be further improved. And the force was also more

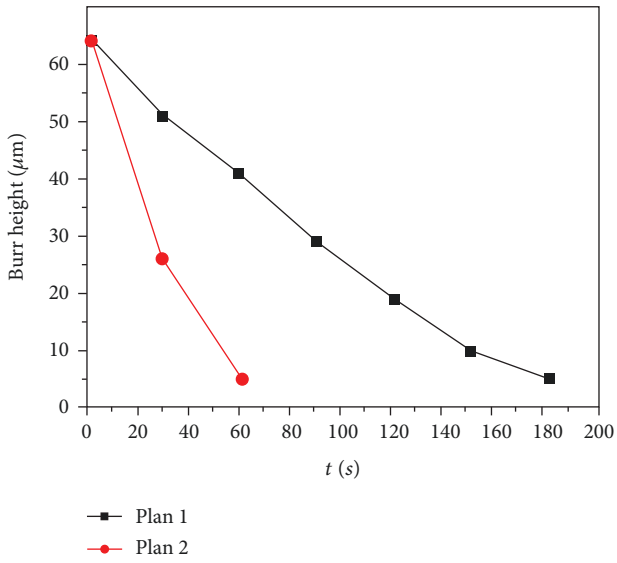

Figure 7: Comparison of burr height in each plan.

directional than that of Plan 1. These versatile finishing forces, which acted on the burr, caused the edge burr to be bent off, worn off, or gradually ground away.

The novel hole-manufacturing process with the combination of the three steps was adopted by the automatic end effector. The consistency of the hole was guaranteed, and the efficiency of manufactured hole was about 70-75 s per hole. The efficiency can be further improved by using more advanced laser equipment and machine tools.

9. Conclusion

Aiming at the heat shield of an aeroengine, a composite hole-manufacturing technology is proposed based on a laser cutting process, a reaming process, and the MAF process. Combining theoretical analysis and experimental research, the main conclusions are as follows:

(1) The best process parameters for laser cutting the base hole of the GH3128 plate are **A** = −0.25 mm; **B** = 200 mm/min; **C** = 210 A; **D** = 0.9 ms; and **E** = 70 Hz. The conclusion of ANOVA was consistent with the result obtained in the intuitive analysis. The factors influencing the effect of the laser cutting process of the GH3128 plate are **D** > **B** > **A** > **E** > **C**.

(2) The edge burr level decreased obviously with the reaming process after the laser cutting process of the base hole. The height and width of the burrs are about 68.4% and 71.1%, respectively, compared to the conventional direct drilling process.

(3) The introduction of the rotation of the main shaft will enable the force of the magnetic brush to have more direction to the edge burrs. This multidirectional finishing force brings higher removal efficiency.

Data Availability

The data used to support the findings of this study are available from the corresponding author upon request.

Conflicts of Interest

The authors declare that they have no conflicts of interest.

Acknowledgments

This paper was supported by the "High-End CNC Machine Tools and Basic Manufacturing Equipment" (2016ZX04002005) of the National Major Science and Technology Projects, China.

References

[1] E. O. Ezugwu, J. Bonney, and Y. Yamane, "An overview of the machinability of aeroengine alloys," *Journal of Materials Processing Technology*, vol. 134, no. 2, pp. 233–253, 2003.

[2] Z. Li, "Progress on effect of processes and microelements on liquation cracking of weld heat-affected zone of nickel-based alloy," *Journal of Mechanical Engineering*, vol. 52, no. 6, p. 37, 2016.

[3] M. G. Xu, J. H. Zhang, Y. Li, Q. H. Zhang, and S. F. Ren, "Material removal mechanisms of cemented carbides machined by ultrasonic vibration assisted EDM in gas medium," *Journal of Materials Processing Technology*, vol. 209, no. 4, pp. 1742–1746, 2009.

[4] G. D'Urso, G. Maccarini, and C. Ravasio, "Process performance of micro-EDM drilling of stainless steel," *The International Journal of Advanced Manufacturing Technology*, vol. 72, no. 9–12, pp. 1287–1298, 2014.

[5] R. Sun, "Characteristic of hole wall trepanning by picosecond laser in superalloy," *Rare Metal Materials & Engineering*, vol. 42, pp. 128–131, 2013.

[6] S. L. Ko, J. E. Chang, and G. E. Yang, "Burr minimizing scheme in drilling," *Journal of Materials Processing Technology*, vol. 140, no. 1–3, pp. 237–242, 2003.

[7] Q. S. Huang, X. J. Gao, W. X. Li, W. LC, and S. JG, "Forming process design and optimization of engine after-burners heat shield in aeronautics field," *Forging & Stamping Technology*, vol. 35, no. 3, pp. 61–65, 2010.

[8] J. C. Bai, *Technology of Non-Traditional Machining*, Harbin Institute of Technology Press, 2015.

[9] Q. Meng, "Vaporization-melt ratio mathematical model and experiments of laser cutting sheet metal," *Journal of Mechanical Engineering*, vol. 47, no. 17, p. 172, 2011.

[10] H. Lei, Z. Yi, and M. Chenglong, "Technological study of laser cutting silicon steel controlled by rotating gas flow," *Optics & Laser Technology*, vol. 41, no. 3, pp. 328–333, 2009.

[11] X. Chen, T. Li, K. zhai, Z. Hu, and M. Zhou, "Using orthogonal experimental method optimizing surface quality of CO_2, laser cutting process for PMMA microchannels," *International Journal of Advanced Manufacturing Technology*, vol. 88, no. 9–12, pp. 2727–2733, 2017.

[12] A. K. Pandey and A. K. Dubey, "Multiple quality optimization in laser cutting of difficult-to-laser-cut material using grey-fuzzy methodology," *International Journal of Advanced*

Manufacturing Technology, vol. 65, no. 1-4, pp. 421–431, 2013.

[13] B. el Aoud, M. Boujelbene, E. Bayraktar, S. Ben Salem, and I. Miskioglu, "Studying effect of CO_2 laser cutting parameters of titanium alloy on heat affected zone and kerf width using the Taguchi method," *Mechanics of Composite and Multi-functional Materials*, vol. 6, pp. 143–150, 2018.

[14] A. E. Gvozdev, et al.I. V. Golyshev, I. V. Minayev et al., "Multiparametric optimization of laser cutting of steel sheets," *Inorganic Materials: Applied Research*, vol. 6, no. 4, pp. 305–310, 2015.

[15] H. Yun, B. Han, Y. Chen, and M. Liao, "Internal finishing process of alumina ceramic tubes by ultrasonic-assisted magnetic abrasive finishing," *International Journal of Advanced Manufacturing Technology*, vol. 85, no. 1-4, pp. 727–734, 2016.

[16] C. T. Lin, L. D. Yang, and H. M. Chow, "Study of magnetic abrasive finishing in free-form surface operations using the Taguchi method," *International Journal of Advanced Manufacturing Technology*, vol. 34, no. 1-2, pp. 122–130, 2007.

[17] G. C. Verma, P. Kala, and P. M. Pandey, "Experimental investigations into internal magnetic abrasive finishing of pipes," *International Journal of Advanced Manufacturing Technology*, vol. 88, no. 5-8, pp. 1657–1668, 2017.

[18] Z. W. du, Y. Chen, K. Zhou, and C. Li, "Research on the electrolytic-magnetic abrasive finishing of nickel-based superalloy GH4169," *International Journal of Advanced Manufacturing Technology*, vol. 81, no. 5-8, pp. 897–903, 2015.

[19] Y. Wang and D. J. Hu, "Design of rotating magnetic field about internal finishing of stainless steel tube," *Chinese Journal of Mechanical Engineering*, vol. 41, no. 2, pp. 102–106, 2005.

[20] J. Anyuan, Q. Hongjun, C. Yan, and H. Bing, "Experimental research of titanium alloy taper hole by ultrasonic magnetic abrasive finishing," *Journal of Mechanical Engineering*, vol. 53, no. 19, pp. 114–119, 2017.

[21] L. Gang, W. Yafei, Z. Heng, G. Kaiye, K. Yinglin, and D. Zuoheng, "Research on helical milling specialized tool based on chip-splitting principle," *Journal of Mechanical Engineering*, vol. 50, no. 9, pp. 176–184, 2014.

[22] H. Wang, X. Qin, D. Wu, and A. Song, "Optimization of cutting parameters in helical milling of carbon fiber reinforced polymer," *Transactions of Tianjin University*, vol. 24, no. 1, pp. 91–100, 2018.

[23] X. Li, F. Bai, and Y. Fu, "The small hole helical mill-grinding process and application in high volume fraction SiCp/Al MMCs," *International Journal of Advanced Manufacturing Technology*, vol. 91, no. 9-12, pp. 3007–3014, 2017.

[24] X. H. Lu, Z. Jia, H. Wang, X. X. Wang, L. K. Si, and L. Gao, "Stability analysis for micro-milling nickel-based superalloy process," *International Journal of Advanced Manufacturing Technology*, vol. 86, no. 9-12, pp. 2503–2515, 2016.